# Reframing Gaussian Splatting Densification with Complexity-Density Consistency of Primitives

Zhemeng Dong, Junjun Jiang, Youyu Chen, Jiaxin Zhang, Kui Jiang, Xianming Liu

Faculty of Computing, Harbin Institute of Technology

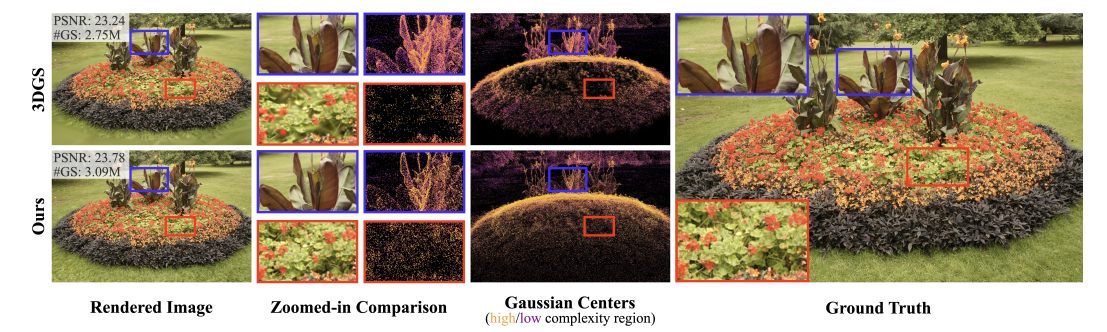


Figure 1: Comparison between vanilla 3DGS and our CDC-GS on the rendering quality and distribution of Gaussian primitives. CDC-GS allocates Gaussian primitives in a more efficient fashion, using more primitives modeling complex region and less to model plain area, and thus significantly improves the rendering quality with a similar level of primitive number.

#### Abstract

The essence of 3D Gaussian Splatting (3DGS) training is to smartly allocate Gaussian primitives, expressing complex regions with more primitives and vice versa. Prior researches typically mark out under-reconstructed regions in a renderingloss-driven manner. However, such a loss-driven strategy is often dominated by low-frequency regions, which leads to insufficient modeling of high-frequency details in texture-rich regions. As a result, it yields a suboptimal spatial allocation of Gaussian primitives. This inspires us to excavate the loss-agnostic visual prior in training views to identify complex regions that need more primitives to model. Based on this insight, we propose Complexity-Density Consistent Gaussian Splatting (CDC-GS), which allocates primitives based on the consistency between visual complexity of training views and the density of primitives. Specifically, primitives involved in rendering high visual complexity areas are categorized as modeling high complexity regions, where we leverage the high frequency wavelet components of training views to measure the visual complexity. And the density of a primitive is computed with the inverse of geometric mean of its distance to the neighboring primitives. Guided by the positive correlation between primitive complexity and density, we determine primitives to be densified as well as pruned. Extensive experiments demonstrate that our CDC-GS surpasses the baseline methods in rendering quality by a large margin using the same amount of Gaussians. And we provide insightful analysis to reveal that our method serves perpendicularly to rendering loss in guiding Gaussian primitive allocation. Our implementations are available on our project page: cdc-gs.github.io.

<sup>\*</sup>Corresponding author. E-mail: jiangjunjun@hit.edu.cn.

# 1 Introduction

3D reconstruction, as a long investigated task of both computer vision and compute graphics communities, aims to build 3D representation of the scene from a batch of posed input views, which can be utilized for novel view synthesis, geometry reconstruction, semantic understanding and other downstream tasks. 3D Gaussian Splatting (3DGS) [1] has emerged as the leading paradigm for this task, offering a compelling combination of photorealistic and real-time rendering performance. Benefiting from explicitly modeling the scene with a set of Gaussian primitives, 3DGS is friendly to graphical rasterization pipeline, and thus being far more efficient than Neural Radiance Fields (NeRF) [2] in novel view synthesis. Recent researches have revealed that the allocation of Gaussian primitives is the key to high quality 3DGS representation [3, 4, 5, 6], referring to the densification and pruning of Gaussian primitives in 3DGS training process.

The training of 3DGS starts with a set of sparse Gaussian primitives, which are then iteratively optimized, densified, and pruned to form a well-distributed and compact representation. Vanilla 3DGS [1] assigns the positional gradient of each Gaussian primitive to themselves as the densification score, and mark out the coarse primitives with a densification score above the densification threshold to be densified. While recent works have explored alternative densification scores beyond positional gradient [7, 4, 5, 8], they are basically driven by rendering loss. Such loss-driven densification schemes typically struggle with expressing high-complexity visual details, where the rendering loss is smoothed out and fails to mark out the coarse Gaussian primitives for densification (Figure 1). Though one can solve this problem by decreasing the densification threshold for more primitives, this will lead to explosive growth of primitives in plain regions. These redundant primitives can barely improve the rendering quality but hinder the rendering efficiency.

Inspired by the fact that the failure of loss-driven densification happens in high visual complexity regions, we argue that we can specify these regions with visual prior measuring the visual complexity. Sparse Gaussian primitives in complex regions should be densified to allocate more primitives to the regions, while the redundant dense primitives in plain regions should be pruned for simplification and efficiency. With this insight, we propose Complexity-Density Consistent Gaussian Splatting (CDC-GS), which serves perpendicularly as a Gaussian primitive allocation method to existing loss-driven ones. Our method measures the visual complexity of training views with the high frequency component of Discrete Wavelet Transform (DWT) [9], and categorizes the primitives involved most with rendering the high frequency areas of training views as modeling complex regions. To measure the density of the neighboring space around a primitive, we utilize the inverse of geometric mean of its distance to the neighboring primitives. Combining the above two measurements, we define a loss-agnostic prior-based densification score, partitioning all primitives into four quadrants, where the two axes are complexity and density of primitives, as shown in Figure 2. Our CDC-GS suppresses the primitives in the left-up and right-down corner (see Figure 4a), which corresponds to the under-reconstructed and over-reconstructed regions, respectively.

To further improve the performance of CDC-GS, we introduce a complexity-aware adaptive densification threshold scheme, which adjusts the densification threshold in a primitive-wise manner. Primitives modeling complex regions are assigned with a lower densification threshold, which helps to allocate more Gaussians to complex regions, and vice versa.

Extensive experiments are performed on standard 3DGS benchmarks, which demonstrate that our method substantially improves the rendering quality with the same level of primitive number compared to baselines. We also provide insightful analysis on why the proposed prior-based primitive allocation strategy are perpendicular to existing loss-based ones, which further advocates the soundness of our method. To summarize our contributions,

- We propose a novel Gaussian primitive allocation scheme based on loss-agnostic visual prior, which
  guides 3DGS to allocate Gaussian primitives smartly by modeling complex regions with dense
  primitives and plain regions with sparse ones.
- We develop Complexity-Density Consistent Gaussian Splatting, which utilizes the wavelet frequency prior and primitive density to detect primitives in under-reconstructed and overreconstructed regions for densification and pruning.
- Insightful analysis is provided to demonstrate why the proposed complexity-density consistent prior serves as a perpendicular primitive allocation strategy against existing loss-driven methods.

# 2 Related Work

**3D Reconstruction.** The target of 3D reconstruction is to obtain high quality 3D representation of the scene. Each time when the representation paradigm evolves always brings a new trend to the research community. Early works use point clouds to reconstruct the scene [10, 11, 12, 13], which remain popular these days in certain domains but struggle to recover textures, failing in novel view synthesis. Alternatively, Neural Radiance Fields (NeRF) [2] represents the scene as an implicit radiance field encoded in a multi-layer perceptron (MLP). While showing significant advantage in novel view synthesis against prior methods, NeRF based reconstruction methods have bottleneck in the efficiency of training and rendering [14, 15, 16, 17]. More recently, 3D Gaussian Splatting (3DGS) [1] emerges as a new leading paradigm for 3D reconstruction, highlighted with fast training and real-time rendering. Over time, numerous extensions have further enhanced its efficiency [8, 18, 19, 20], compactness [21, 22, 23, 24], and robustness under challenging conditions [25, 26, 27, 28, 29]. Using a set of 3D Gaussian primitives expressing the scene, 3DGS can be adopted to extensive tasks, such as novel view synthesis [30, 31, 32, 33], geometric reconstruction [34, 35, 36, 37, 38], 3D segmentation [39, 40, 41], and semantic understanding [42, 43, 44, 45].

Primitive Allocation for 3DGS. To obtain high quality 3DGS representation of the scene, it is vital to correctly allocate Gaussian primitives over the space. The allocation is expected to use more primitives to model the complex regions and less primitives to model the plain regions. For primitive densification, prior works propose different densification scores to measure if a primitive is modeling an under-reconstructed region. Vanilla 3DGS [1] adopts high positional gradient of primitives centers derived from the rendering loss as the densification score. Absgs [4] takes a step forward by calculating the sum of pixel-wise absolute gradient, addressing the conflicts in gradient direction of vanilla 3DGS [1]. Revising-3DGS [7] utilizes the primitive-involved high rendering error instead, which differs from positional gradient but is still driven by the rendering loss. Taming-3DGS [8] proposes a densification score mixing primitive attributes and positional gradient. All of these methods specifies under-reconstructed primitives in a loss-driven manner, thus they are either struggled with under-reconstruction in complex regions (vanilla 3DGS, Revising-3DGS, Taming-3DGS) or over-reconstruction in plain regions (Absgs). On the other hand, redundant primitives are pruned to slim the primitives. The most widely adopted metric is to prune primitives with low opacity [46, 47, 48]. There are also methods pruning the primitives with over-dense neighbors [3, 21].

Frequency-based 3DGS Densification. Since our work use frequency information of training views to guide the allocation of Gaussian primitives, we specifically introduce the works investigating the use of frequency theory for primitive allocation. FreGS [49] improves 3DGS optimization with loss in frequency domain, but at the cost of explosive primitive growth, resulting in two times of primitives compared to 3DGS. Although FDS-GS [50] proposes a frequency-aware density control method, they mainly focus on the connection between density and scale of primitives and do not really investigate how visual frequency impacts 3DGS. Compared to them, our method explicitly utilize the frequency information in training views as a prior to guide the densification, addressing the under-reconstruction and over-reconstruction in a simple and efficient scheme. Furthermore, we provide experimental evidence to prove that our method perpendicularly discovers under-reconstructed Gaussian primitives ignored by prior loss-driven method, which further emphasizes the superiority of our method.

# 3 Method

In this section, we introduce our CDC-GS in detail. In Section 3.1, we first review preliminaries about 3D Gaussian Splatting and Discrete Wavelet Transform. In Section 3.2, we introduce how CDC-GS computes the complexity and density of Gaussian primitives. In Section 3.3, we explain how CDC-GS utilizes complexity-density consistency to specify coarse and redundant primitives in under-reconstructed and over-reconstructed regions, which is the key of our method to allocate Gaussian primitives based on loss-agnostic visual prior.

# 3.1 Preliminary

#### 3.1.1 3D Gaussian Splatting

3D Gaussian Splatting (3DGS) represents a 3D scene using a set of Gaussian primitives  $\{G_i\}_{i=1}^N$ , where N is the number of primitives. Each primitive  $G_i$  is a 3D Gaussian distribution, parameterized

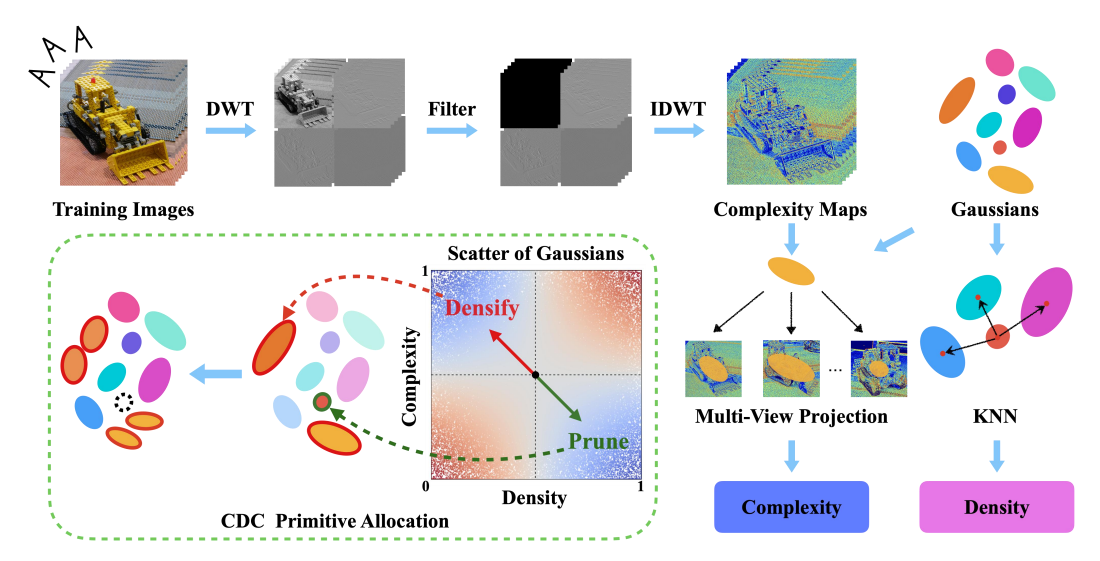


Figure 2: **Overview of our Complexity-Density Consistent Primitive Allocation.** We extract complexity maps for training images using DWT and back-projected the complexity maps onto Gaussian primitives to parameterize their complexity, while the density of each primitive is estimated with geometrical statistics about its neighbors. By densifying the primitives with low density vs. high complexity and pruning the primitives with high density vs. low complexity, CDC-GS adaptively allocates Gaussian primitives across the scene based on complexity of the space.

by its center  $\mu_i \in \mathbb{R}^3$ , opacity  $o_i \in \mathbb{R}^1$ , a full 3D covariance matrix  $\Sigma_i \in \mathbb{R}^{3 \times 3}$ , and Spherical Harmonic (SH) coefficients  $c_i^{\mathrm{sh}} \in \mathbb{R}^{3 \times 16}$  encoding anisotropic appearance. The probability density function of the primitive is defined as,

$$G_i(x) = \exp\left(-\frac{1}{2}(x - \mu_i)^{\top} \Sigma_i^{-1}(x - \mu_i)\right),$$
 (1)

where  $x \in \mathbb{R}^3$  is an arbitrary point in 3D space. For rendering, primitives are projected to the image plane as 2D Gaussians  $G_i^{\text{2D}}$ , and the color  $C(x') \in \mathbb{R}^3$  of a pixel  $x' \in \mathbb{R}^2$  is rasterized as,

$$C(x') = \sum_{j=1}^{P} c_j \alpha_j T_j, \quad \alpha_j = o_j G_j^{2D}(x'), \quad T_j = \prod_{k=1}^{j-1} (1 - \alpha_k),$$
 (2)

where P is the number of primitives covering pixel x', and  $c_j$  is the response of  $c_j^{\rm sh}$  to the current camera view. The optimization of primitives is supervised with color rendering loss [1].

Besides the numerical optimization for primitives, the vanilla 3DGS adopts adaptive primitive allocation to express the scene better. Primitives receiving a positional gradient beyond threshold  $\tau_{\rm pos}$  from the rendering loss are recognized as underfitting, and are densified to allocate more primitive to the region. Meanwhile, primitives possessing low opacity contribute little to modeling the scene according to Equation 2, which are pruned to reduce the primitive redundancy.

#### 3.1.2 Discrete Wavelet Transform

2D Discrete Wavelet Transform (DWT) [9] is a potent tool to analyze frequency information of images. DWT decomposes an image into multiple sub-bands using a pair of orthogonal low-pass and high-pass filters, denoted by  $F_L$  and  $F_H$ , respectively. Given a one-channel image  $I \in \mathbb{R}^{H \times W}$ , where H and W denote height and width of the image, one-level 2D Haar wavelet decomposition is formulated as,

$$DWT(I) = \begin{bmatrix} I^{LL} & I^{LH} \\ I^{HL} & I^{HH} \end{bmatrix} = \begin{bmatrix} F_{L} \\ F_{H} \end{bmatrix} I \begin{bmatrix} F_{L}^{\top} & F_{H}^{\top} \end{bmatrix}.$$
 (3)

Here,  $I^{\rm LL}$ ,  $I^{\rm HH}$ ,  $I^{\rm HL}$ ,  $I^{\rm HH}$  are four sub components of I decomposed by DWT, where  $I^{\rm LL}$  denotes the low-frequency structure (e.g., plain areas) and the rest three components correspond to high-frequency structure of the image (e.g., complex areas and edges). Moreover, DWT is an invertible transformation, which means one can obtain image I with its four sub-components, as  $I = {\rm IDWT}(I^{\rm LL}, I^{\rm LH}, I^{\rm HL})$ .

#### 3.2 Complexity and Density of Gaussian Primitives

Before introducing how our CDC-GS allocates Gaussian primitives with complexity-density consistency prior, we first define the complexity and density of each Gaussian primitive in this section.

The complexity of a primitive is to measure whether it's modeling a complex region, and we excavate this information from the frequency information of training views. We apply DWT to each training view I and break it down into four sub-components, as defined in Equation 3. By removing the low frequency component  $I^{LL}$  and retain the other three components, we extract the high frequency part of image I. And we define the complexity map of image I as,

$$E_I = \text{IDWT}(0, I^{\text{LH}}, I^{\text{HL}}, I^{\text{HH}}), \tag{4}$$

which back projected to Gaussian primitives to compute the complexity of each primitive. Specifically, given a primitive  $G_i$  involved to rendering pixel x' with weight  $w_i(x') = \alpha_i T_i$ , the complexity of  $G_i$  with respect to x' is defined as  $\gamma(G_i, x') = E_I(x') \cdot w_i(x') / \max_{j=1}^P (w_j(x'))$ , where P takes the same meaning as in Equation 2 and the max operator enumerates all the primitives covering x' as normalization. Considering all  $\gamma(G_i, \cdot)$ , which is to enumerate all pixels covered by  $G_i$  in all training views  $\{I\}$ , we take the maximum complexity to represent the complexity of  $G_i$ , which is formulated as,

$$\Gamma(G_i) = \max_{I_v \in \{I\}} \left( \max_{x' \in I_v} \left( \gamma(G_i, x') \right) \right). \tag{5}$$

The definition of  $\gamma$  ensures that the complex areas in training views mainly affect the complexity of the primitives involved most in their rendering, and suppress their influence to the invisible primitives from the view.

Complexity alone cannot affirm if a primitive is in a under-reconstructed region or an over-reconstructed region. For example, high complexity region filled with dense Gaussian primitives is probably well reconstructed, while sparse primitives in such region typically indicate under-reconstruction, which can be ignored by loss-driven indicators such as gradient when the rendering loss is smoothed out with the high-frequency details. It's of necessity to cooperatively take both complexity and density of primitives to specify under-reconstruction and over-reconstruction. To estimate the density of the neighboring space of a primitive  $G_i$ , we compute the inverse of geometric mean of the center distance between  $G_i$  and its neighbors, formulated as,

$$\Psi(G_i) = \left(\prod_{j \in \mathcal{N}_i} ||\mu_i - \mu_j||\right)^{-\frac{1}{|\mathcal{N}_i|}},\tag{6}$$

where  $\mathcal{N}_i$  is the set of nearest neighbors of  $G_i$ . Both formulations are empirically validated to yield more stable and efficient primitive allocation (see Appendix B.1-B.2).

#### 3.3 Complexity-Density Consistent Primitive Allocation

With the complexity and density of Gaussian primitive defined in Section 3.2, we can now introduce how the proposed CDC-GS allocates primitives based on them. As already discussed, the complexity and density of primitive are expected to share consistency in well-reconstructed region, otherwise it could indicate possibility of under-reconstruction or over-reconstruction. To formulate the consistency between the complexity and density of primitive  $G_i$ , we use the production of their normalized value,

$$s_i = \frac{\Gamma(G_i) - \Gamma_{\text{mean}}}{\Gamma_{\text{std}}} \cdot \frac{\Psi(G_i) - \Psi_{\text{mean}}}{\Psi_{\text{std}}},\tag{7}$$

where  $\Gamma_{\text{mean}}$ ,  $\Psi_{\text{mean}}$  are the mean of complexity and density of all primitive respectively, and  $\Gamma_{\text{std}}$ ,  $\Psi_{\text{std}}$  denote the corresponding standard derivation. Positive value of  $s_i$  indicates the consistency of complexity and density, while low complexity vs. high density and high complexity vs. low density results in negative  $s_i$ , indicating over-reconstruction and under-reconstruction respectively.

Our complexity-density consistency serves as a perpendicular complementary to existing primitive allocation method. Denoting primitives selected densified in a certain optimization step as  $\mathcal{M}$ , CDC-GS decomposes  $\mathcal{M}$  into  $\mathcal{M}_{loss}$  and  $\mathcal{M}_{cdc}$ , where  $\mathcal{M} = \mathcal{M}_{loss} \cup \mathcal{M}_{cdc}$ .  $\mathcal{M}_{loss}$  refers to the primitives selected by existing loss-driven densification method (e.g., positional gradient), and  $\mathcal{M}_{cdc}$ 

Table 1: **Quantitative comparison on novel view synthesis.** Results are reproduced with the official implementation of baselines. **Bold** indicates the best results. Our method consistently achieves superior performance across datasets with a fewer or comparable number of Gaussian primitives.

Method		MipNeRI	F 360[30]		Ta	anks & Te	emples[51]	]	Deep Blending[52]			
	PSNR ↑	SSIM↑	LPIPS ↓	#GS↓	PSNR ↑	SSIM ↑	LPIPS ↓	#GS↓	PSNR ↑	SSIM ↑	LPIPS ↓	#GS ↓
3DGS[1]	27.79	0.826	0.201	2.59M	23.79	0.853	0.170	1.57M	29.73	0.906	0.238	2.47M
Taming-3DGS[8]	27.91	0.821	0.211	2.53M	24.32	0.862	0.157	1.60M	29.73	0.908	0.234	2.07M
Ours (0.01)	28.02	0.836	0.183	2.53M	24.42	0.866	0.149	1.60M	29.84	0.909	0.234	2.07M
AbsGS[4]	27.72	0.835	0.169	4.06M	23.22	0.856	0.152	1.90M	29.28	0.903	0.233	3.13M
Mini-Splatting-D[3]	27.78	0.841	0.163	4.61M	23.31	0.855	0.141	4.27M	29.93	0.907	0.210	4.63M
Pixel-GS[5]	27.84	0.835	0.176	5.27M	23.66	0.856	0.150	4.50M	28.95	0.896	0.247	4.65M
Ours (0.02)	28.11	0.842	0.164	3.95M	24.47	0.867	0.140	2.56M	30.03	0.912	0.218	2.49M

denotes the primitives selected by the proposed complexity-density consistency. For the primitives in under-reconstructed regions, we randomly sample up to  $\rho_{\rm d} \cdot N$  of them for densification, where the sampling probability is determined with  $|s_i|$ . For the primitives in over-reconstructed regions, we randomly sample up to  $\rho_{\rm p} \cdot N$  of them to be pruned, where the sampling probability is determined with  $o_i$ . The original pruning strategy of 3DGS at every 100 steps is removed, which is alternated to pruning all primitives with opacity below 0.1 for every 3000 steps.

To further improve the quality of  $\mathcal{M}_{loss}$ , relieving more primitives from under-reconstruction, we propose to adjust the densification threshold of each Gaussian primitive based on its complexity. The complexity-aware densification threshold is defined as,

$$\tau(\Gamma) = \tau_{\text{low}} + (\tau_{\text{upp}} - \tau_{\text{low}}) \cdot [1 - \sigma(\lambda \cdot \Gamma)], \qquad (8)$$

where  $\tau_{\text{low}}$  and  $\tau_{\text{upp}}$  are the lower and upper bound of the densification threshold, respectively.  $\sigma$  refers to the Sigmoid function, and  $\lambda$  is a hyper-parameter.

# 4 Experiments

#### 4.1 Experimental Settings

**Dataset.** We evaluate our method on the real-world datasets widely adopted in novel view synthesis. Specifically, we follow the standard protocol in vanilla 3DGS [1], using 9 scenes from the MipNeRF-360 [30] dataset, the playroom and drjohnson scenes from Deep Blending [52] dataset, and the train and truck scenes from Tanks & Temples [51] dataset. The preprocess of training data also strictly follows vanilla 3DGS [1].

**Metrics.** We report quantitative results with three standard metrics: Peak Signal-to-Noise Ratio (PSNR), Structural Similarity Index Metrics (SSIM) [53] and Learned Perceptual Image Patch Similarity (LPIPS) [54]. All metrics are computed on test views using the original evaluation protocol. We report the average score across all scenes for each dataset. Each experiment is repeated three times with different seeds, and we report the average performance across runs to account for randomness.

**Baselines.** We compare our method with representative methods investigating Gaussian primitive allocation, including vanilla 3DGS[1], Taming-3DGS[8] (constrained to the same number of primitives to our  $\rho_d = 0.01$  version), AbsGS[4] (with the densification threshold set to 0.0004, the dense version of [4]), Mini-Splatting[3] (densification-only version without pruning), and Pixel-GS[5]. All baseline results are reproduced using the official implementations and default configurations to ensure fairness of experiments.

Implementation Details. Our method is implemented on top of the official 3DGS codebase [1]. We extract complexity map of input views using one-level Haar DWT. And the density of Gaussian primitives is computed with 3 nearest neighbors, which is to say  $|\mathcal{N}_i| = 3$  for all primitives. We set  $\rho_d = 0.01$  and  $\rho_p = 0.01$  by default. We also evaluate an additional setting by increasing the splitting ratio to  $\rho_d = 0.02$ . Our complexity-aware densification threshold is configured with  $\tau_{\text{low}} = 1.5 \times 10^{-4}$ ,  $\tau_{\text{upp}} = 2 \times 10^{-4}$  and  $\lambda = 6$ . Other hyper-parameters are consistent with the vanilla 3DGS [1]. All experiments are performed on a single NVIDIA RTX 3090 GPU.

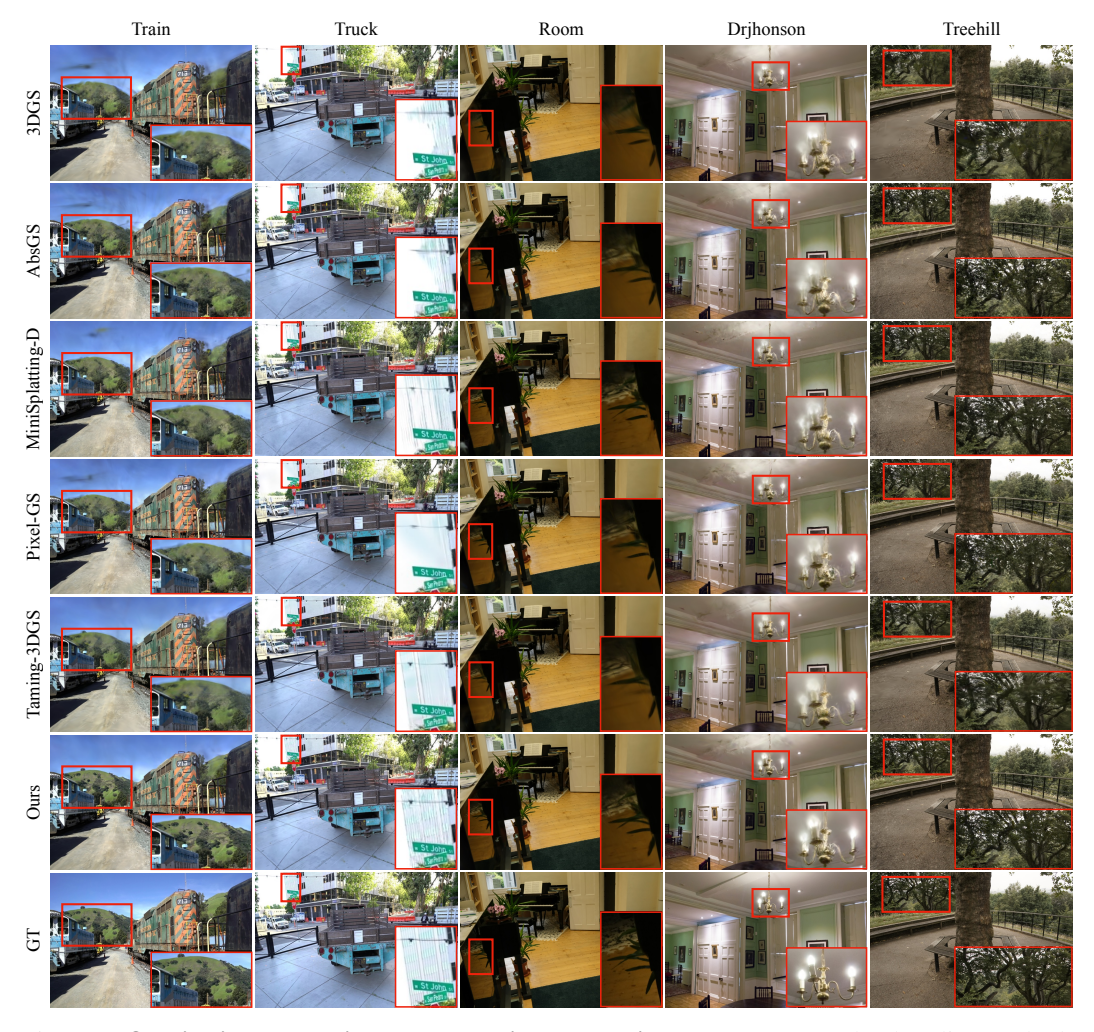


Figure 3: **Qualitative comparison on novel view synthesis results.** Compared to baseline methods, our method yields sharper textures, more faithful structures, and fewer artifacts without increasing primitives, which is attributed to our CDC strategy that improves the allocation of primitives.

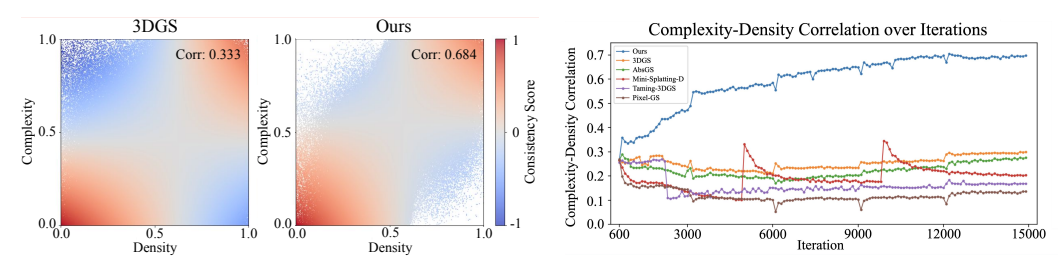
#### 4.2 Comparison to Baseline Methods

Quantitative Comparison. We report quantitative comparison between our CDC-GS and baseline methods in Table 1, where methods with approximate primitive number are grouped together for fair comparison. In the sparse group, CDC-GS ( $\rho_{\rm d}=0.01$ ) consistently outperforms baselines, demonstrating superior fidelity and perceptual quality without increasing the number of primitives. In the dense group, we set  $\rho_{\rm d}=0.02$  to match the primitive number of baselines, ensuring a fair and meaningful comparison. While utilizing fewer primitives in general, CDC-GS achieves the best rendering quality across all benchmarks. The results further validate that our proposed complexity-density consistent allocation strategy enables more precise modeling of intricate structures while improving primitive allocation efficiency.

**Qualitative Analysis.** We show qualitative comparisons corresponding to Table 1 across various scenes in Figure 3. Our method consistently presents more detailed textures, cleaner structural boundaries, and fewer artifacts. The results advocates that our method success to discover the under-reconstructed regions that the baseline methods tend to overlook.

#### 4.3 CDC as a Perpendicular Densification Indicator to Rendering Loss

In this subsection, we reveal that the proposed complexity-density consistency serves as a perpendicular indicator against the loss-driven ones to specify the under-reconstructed regions.



- (a) Complexity-density map of primitives.
- (b) Complexity-density correlation along densification.

Figure 4: Analysis for complexity-density consistency on the scene "kitchen" of MipNeRF-360 dataset [30]. (a) The scatters depict the primitives at the end of densification (15k iteration) for 3DGS and our CDC-GS, with each primitive localized by its density and complexity. The color of each primitive indicates its consistency score  $s_i$  (see Equation 7). The overall Pearson correlation [55] of complexity and density of primitives is shown at top-right. Color in the two scatters are normalized and aligned to ensure the same color corresponds to the same consistency score value. (b) Variation of complexity-density Pearson correlation over the densification progress (600–15k iteration).

In Figure 4a, we present two scatter diagrams for vanilla 3DGS [1] and CDC-GS, with all Gaussian primitives represented by their complexity and density. The scatters show the degree of the primitives in the optimized 3DGS model of scene "kitchen" matching the rule of complexity-density consistency. While vanilla 3DGS exhibits little consistency in complexity and density, CDC-GS significantly reduces the primitives in the left-up and right-down corner, which indicates the most inconsistent primitives are remove with our proposed primitive allocation strategy. Accompanied with Table 1 and Figure 3, we can draw the conclusion that the reduction of primitives in these regions do contribute to the quality of 3DGS model.

Moreover, in Figure 4b, we also provide the variation of complexity-density consistency along the training process of CDC-GS and all the baselines on the scene "kitchen". We use Pearson correlation [55] to evaluate the overall consistency between the complexity and density over all Gaussian primitives, which is to evaluate the degree of scatters in Figure 4 constrained in the first and the third quadrant. While CDC-GS performs a consistent increase in the consistency, baseline methods fail to largely improve the consistency alone the training process. Notably, slight improvement in the consistency of the baseline methods can be observed along the training process, which demonstrates that the complexity-density consistency naturally relates to the optimization of 3DGS, but struggles to improve without explicit manipulation. This advocates that the complexity-density consistency is perpendicular to loss-driven densification indicators.

To further consolidate this conclusion, we categorize the primitives in of vanilla 3DGS (left of Figure 4a) into two groups with the positional gradient of primitives and the densification threshold, which is presented in Figure 5a. We perform the same operation to AbsGS [4] and show the result in Figure 5b. The color of primitives indicates their positional gradient. Patterns can be barely drawn by splitting the primitives with the densification threshold, demonstrating that coarse primitives recognized with positional gradient ( $\mathcal{M}_{loss}$ , see Section 3.3) doesn't contain the primitives recognized with complexity-density consistency ( $\mathcal{M}_{cdc}$ ), which is to say that  $\mathcal{M}_{cdc}$  shares little cross with  $\mathcal{M}_{loss}$ . We believe the above experiment results are convincing enough to support the perpendicularity of complexity-density consistency against loss-driven densification indicators.

#### 4.4 Ablations

We perform ablation studies on the Tanks & Temples dataset [51] using the vanilla 3DGS [1] as backbone to assess the individual contributions of the proposed Complexity-Aware Adaptive Threshold (CAAT) and Complexity-Density Consistency (CDC) introduced in Section 3.3. Result is summarized in Table 2.

**Ablation on CAAT.** CAAT improves the reconstruction quality by manipulating densification threshold with complexity of Gaussian primitives. Slight increase in the number of primitives is observed because of aggressive densification in complex areas.

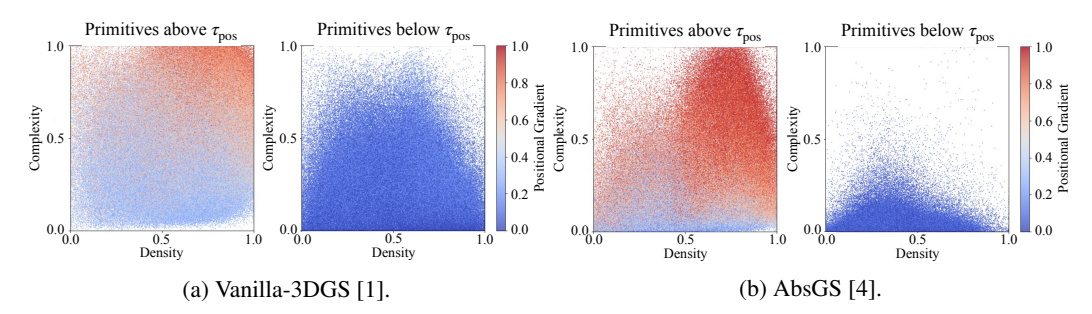


Figure 5: **Perpendicularity between complexity-density consistency and positional gradient.** We breakdown Figure 4a, categorizing the Gaussian primitives into two groups by if their positional gradient are above the densification threshold or not. And we show the same statistical information for AbsGS in Figure 5b. Color of primitives indicates the normalized magnitude of positional gradient. Primitives are categorized in a complexity-density consistency agnostic way, advocating that the proposed complexity-density consistency is perpendicular to the loss-driven positional gradient.

Table 2: **Ablation study on Tanks & Temples dataset.** We evaluate the contribution of the proposed modules: Complexity-Aware Adaptive Threshold (CAAT) and Complexity-Density Consistency (CDC). The full method (CDC-GS) combines both.

Method	PSNR ↑	SSIM↑	LPIPS ↓	#GS↓
3DGS	23.79	0.853	0.170	1.57M
3DGS + CAAT	24.00	0.859	0.163	1.70M
3DGS + CDC	24.22	0.862	0.153	1.51M
CDC-GS (Ours)	24.42	0.866	0.149	1.60M

**Ablation on CDC.** CDC achieves a substantial gain by simultaneous densification in under-reconstructed region and pruning in over-reconstructed region. Improvement in visual quality demonstrates that the proposed CDC strategy successfully mitigates the under-reconstructed problem in vanilla 3DGS[1], while the concurrent reduction of Gaussian primitives confirms its effectiveness in eliminating unnecessary primitives in low-complexity regions.

**Full Method.** When combining CAAT and CDC, the two modules act synergistically: CAAT introduces complexity-aware densification to refine local details, while CDC enforces global complexity-density consistency by adjusting the primitive distribution according to the complexity of the scene. As a result, CDC-GS significantly improve the reconstruction quality while maintaining a Gaussian primitive count comparable to the vanilla 3DGS[1], demonstrating the strength of the proposed Gaussian primitive allocation strategy.

#### 5 Conclusion

In this paper, we propose CDC-GS, a novel Gaussian primitive allocation method, which is perpendicular to existing loss-driven ones, such as the ones using positional gradient. Our method explores the under-reconstructed region with high complexity and low density, and the over-reconstructed region with low complexity and high density. Extensive experiments are performed to demonstrate the superiority of our method and its perpendicularity to existing primitive allocation methods. It's power is fully played as a complementary to existing loss-driven primitive allocation methods. We believe it is valuable for finding the sub-optimally reconstructed regions ignored by existing methods in a prior driven manner.

**Limitations.** While improving Gaussian primitive allocation from an orthogonal perspective, our method still requires existing loss-driven cues (e.g., positional gradients), as the visual prior itself lacks direct awareness of reconstruction quality. In future work, we plan to further investigate how visual priors influence primitive allocation, toward more coherent and adaptive allocation strategies.

# Acknowledgments

The research was supported by the National Natural Science Foundation of China (U23B2009, 62471158).

#### References

- [1] B. Kerbl, G. Kopanas, T. Leimkühler, and G. Drettakis, "3D Gaussian Splatting for Real-Time Radiance Field Rendering." *ACM Trans. Graph.*, vol. 42, no. 4, pp. 139–1, 2023.
- [2] B. Mildenhall, P. P. Srinivasan, M. Tancik, J. T. Barron, R. Ramamoorthi, and R. Ng, "NeRF: Representing Scenes as Neural Radiance Fields for View Synthesis," *Communications of the ACM*, vol. 65, no. 1, pp. 99–106, 2021.
- [3] G. Fang and B. Wang, "Mini-Splatting: Representing Scenes with a Constrained Number of Gaussians," in *European Conference on Computer Vision*. Springer, 2024, pp. 165–181.
- [4] Z. Ye, W. Li, S. Liu, P. Qiao, and Y. Dou, "AbsGS: Recovering Fine Details in 3D Gaussian Splatting," in *Proceedings of the 32nd ACM International Conference on Multimedia*, 2024, pp. 1053–1061.
- [5] Z. Zhang, W. Hu, Y. Lao, T. He, and H. Zhao, "Pixel-GS: Density Control with Pixel-Aware Gradient for 3D Gaussian Splatting," in *European Conference on Computer Vision*. Springer, 2024, pp. 326–342.
- [6] X. Deng, C. Diao, M. Li, R. Yu, and D. Xu, "Efficient Density Control for 3D Gaussian Splatting," arXiv preprint arXiv:2411.10133, 2024.
- [7] S. Rota Bulò, L. Porzi, and P. Kontschieder, "Revising Densification in Gaussian Splatting," in *European Conference on Computer Vision*. Springer, 2024, pp. 347–362.
- [8] S. S. Mallick, R. Goel, B. Kerbl, M. Steinberger, F. V. Carrasco, and F. De La Torre, "Taming 3DGS: High-Quality Radiance Fields with Limited Resources," in SIGGRAPH Asia 2024 Conference Papers, ser. SA '24. New York, NY, USA: Association for Computing Machinery, 2024. [Online]. Available: https://doi.org/10.1145/3680528.3687694
- [9] I. Daubechies, Ten Lectures on Wavelets. SIAM, 1992.
- [10] J. P. Grossman and W. J. Dally, "Point Sample Rendering," in *Rendering Techniques' 98: Proceedings of the Eurographics Workshop in Vienna, Austria, June 29—July 1, 1998 9.* Springer, 1998, pp. 181–192.
- [11] J. Wu and L. Kobbelt, "Optimized Sub-Sampling of Point Sets for Surface Splatting," in *Computer Graphics Forum*, vol. 23, no. 3. Wiley Online Library, 2004, pp. 643–652.
- [12] L. Kobbelt and M. Botsch, "A survey of point-based techniques in computer graphics," Computers & Graphics, vol. 28, no. 6, pp. 801–814, 2004.
- [13] M. Gross and H. Pfister, *Point-based Graphics*. Elsevier, 2011.
- [14] A. Yu, V. Ye, M. Tancik, and A. Kanazawa, "pixelNeRF: Neural Radiance Fields From One or Few Images," in *Proceedings of the IEEE/CVF conference on computer vision and pattern recognition*, 2021, pp. 4578–4587.
- [15] S. Fridovich-Keil, A. Yu, M. Tancik, Q. Chen, B. Recht, and A. Kanazawa, "Plenoxels: Radiance Fields Without Neural Networks," in *Proceedings of the IEEE/CVF conference on computer vision and pattern recognition*, 2022, pp. 5501–5510.
- [16] A. Chen, Z. Xu, A. Geiger, J. Yu, and H. Su, "TensoRF: Tensorial Radiance Fields," in *European conference on computer vision*. Springer, 2022, pp. 333–350.
- [17] T. Müller, A. Evans, C. Schied, and A. Keller, "Instant neural graphics primitives with a multiresolution hash encoding," *ACM transactions on graphics (TOG)*, vol. 41, no. 4, pp. 1–15, 2022.
- [18] Z. Fan, K. Wang, K. Wen, Z. Zhu, D. Xu, Z. Wang et al., "LightGaussian: Unbounded 3D Gaussian Compression with 15x Reduction and 200+ FPS," Advances in neural information processing systems, vol. 37, pp. 140 138–140 158, 2024.
- [19] G. Feng, S. Chen, R. Fu, Z. Liao, Y. Wang, T. Liu, B. Hu, L. Xu, Z. Pei, H. Li et al., "FlashGS: Efficient 3D Gaussian Splatting for Large-scale and High-resolution Rendering," in *Proceedings of the Computer Vision and Pattern Recognition Conference*, 2025, pp. 26 652–26 662.
- [20] Y. Chen, J. Jiang, K. Jiang, X. Tang, Z. Li, X. Liu, and Y. Nie, "DashGaussian: Optimizing 3D Gaussian Splatting in 200 Seconds," in *Proceedings of the Computer Vision and Pattern Recognition Conference*, 2025, pp. 11146–11155.
- [21] P. Papantonakis, G. Kopanas, B. Kerbl, A. Lanvin, and G. Drettakis, "Reducing the Memory Footprint of 3D Gaussian Splatting," *Proceedings of the ACM on Computer Graphics and Interactive Techniques*, vol. 7, no. 1, pp. 1–17, 2024.

- [22] T. Lu, M. Yu, L. Xu, Y. Xiangli, L. Wang, D. Lin, and B. Dai, "Scaffold-GS: Structured 3D Gaussians for View-Adaptive Rendering," in *Proceedings of the IEEE/CVF Conference on Computer Vision and Pattern Recognition*, 2024, pp. 20654–20664.
- [23] K. Ren, L. Jiang, T. Lu, M. Yu, L. Xu, Z. Ni, and B. Dai, "Octree-GS: Towards Consistent Real-time Rendering with LOD-Structured 3D Gaussians," *arXiv preprint arXiv:2403.17898*, 2024.
- [24] S. Niedermayr, J. Stumpfegger, and R. Westermann, "Compressed 3D Gaussian Splatting for Accelerated Novel View Synthesis," in *Proceedings of the IEEE/CVF Conference on Computer Vision and Pattern Recognition*, 2024, pp. 10349–10358.
- [25] J. Tang, J. Ren, H. Zhou, Z. Liu, and G. Zeng, "DreamGaussian: Generative Gaussian Splatting for Efficient 3D Content Creation," arXiv preprint arXiv:2309.16653, 2023.
- [26] J. Oh, J. Chung, D. Lee, and K. M. Lee, "DeblurGS: Gaussian Splatting for Camera Motion Blur," arXiv preprint arXiv:2404.11358, 2024.
- [27] Z. Yang, X. Gao, W. Zhou, S. Jiao, Y. Zhang, and X. Jin, "Deformable 3D Gaussians for High-Fidelity Monocular Dynamic Scene Reconstruction," in *Proceedings of the IEEE/CVF conference on computer vision and pattern recognition*, 2024, pp. 20331–20341.
- [28] Z. Yang, X. Gao, Y.-T. Sun, Y. Huang, X. Lyu, W. Zhou, S. Jiao, X. Qi, and X. Jin, "Spec-Gaussian: Anisotropic View-Dependent Appearance for 3D Gaussian Splatting," *Advances in Neural Information Processing Systems*, vol. 37, pp. 61 192–61 216, 2024.
- [29] G. Wu, T. Yi, J. Fang, L. Xie, X. Zhang, W. Wei, W. Liu, Q. Tian, and X. Wang, "4D Gaussian Splatting for Real-Time Dynamic Scene Rendering," in *Proceedings of the IEEE/CVF conference on computer vision* and pattern recognition, 2024, pp. 20310–20320.
- [30] J. T. Barron, B. Mildenhall, D. Verbin, P. P. Srinivasan, and P. Hedman, "Mip-NeRF 360: Unbounded Anti-Aliased Neural Radiance Fields," in *Proceedings of the IEEE/CVF conference on computer vision* and pattern recognition, 2022, pp. 5470–5479.
- [31] Z. Zhu, Z. Fan, Y. Jiang, and Z. Wang, "FSGS: Real-Time Few-Shot View Synthesis Using Gaussian Splatting," in *European conference on computer vision*. Springer, 2024, pp. 145–163.
- [32] D. Charatan, S. L. Li, A. Tagliasacchi, and V. Sitzmann, "pixelSplat: 3D Gaussian Splats from Image Pairs for Scalable Generalizable 3D Reconstruction," in *Proceedings of the IEEE/CVF conference on computer* vision and pattern recognition, 2024, pp. 19457–19467.
- [33] X. Liu, Z. Huang, F. Okura, and Y. Matsushita, "HoGS: Unified Near and Far Object Reconstruction via Homogeneous Gaussian Splatting," *arXiv preprint arXiv:2503.19232*, 2025.
- [34] A. Guédon and V. Lepetit, "SuGaR: Surface-Aligned Gaussian Splatting for Efficient 3D Mesh Reconstruction and High-Quality Mesh Rendering," in *Proceedings of the IEEE/CVF Conference on Computer Vision and Pattern Recognition*, 2024, pp. 5354–5363.
- [35] B. Huang, Z. Yu, A. Chen, A. Geiger, and S. Gao, "2D Gaussian Splatting for Geometrically Accurate Radiance Fields," in *ACM SIGGRAPH 2024 conference papers*, 2024, pp. 1–11.
- [36] Z. Yu, T. Sattler, and A. Geiger, "Gaussian Opacity Fields: Efficient Adaptive Surface Reconstruction in Unbounded Scenes," *ACM Transactions on Graphics (ToG)*, vol. 43, no. 6, pp. 1–13, 2024.
- [37] B. Zhang, C. Fang, R. Shrestha, Y. Liang, X. Long, and P. Tan, "RaDe-GS: Rasterizing Depth in Gaussian Splatting," arXiv preprint arXiv:2406.01467, 2024.
- [38] D. Chen, H. Li, W. Ye, Y. Wang, W. Xie, S. Zhai, N. Wang, H. Liu, H. Bao, and G. Zhang, "PGSR: Planar-Based Gaussian Splatting for Efficient and High-Fidelity Surface Reconstruction," *IEEE Transactions on Visualization and Computer Graphics*, 2024.
- [39] X. Hu, Y. Wang, L. Fan, J. Fan, J. Peng, Z. Lei, Q. Li, and Z. Zhang, "Semantic Anything in 3D Gaussians," CoRR, 2024.
- [40] Q. Shen, X. Yang, and X. Wang, "FlashSplat: 2D to 3D Gaussian Splatting Segmentation Solved Optimally," in European Conference on Computer Vision. Springer, 2024, pp. 456–472.
- [41] J. Zhang, J. Jiang, Y. Chen, K. Jiang, and X. Liu, "COB-GS: Clear Object Boundaries in 3DGS Segmentation Based on Boundary-Adaptive Gaussian Splitting," in CVPR, 2025.
- [42] J. Guo, X. Ma, Y. Fan, H. Liu, and Q. Li, "Semantic Gaussians: Open-Vocabulary Scene Understanding with 3D Gaussian Splatting," arXiv preprint arXiv:2403.15624, 2024.
- [43] M. Ye, M. Danelljan, F. Yu, and L. Ke, "Gaussian Grouping: Segment and Edit Anything in 3D Scenes," in *European Conference on Computer Vision*. Springer, 2024, pp. 162–179.
- [44] J.-C. Shi, M. Wang, H.-B. Duan, and S.-H. Guan, "Language Embedded 3D Gaussians for Open-Vocabulary Scene Understanding," in *Proceedings of the IEEE/CVF Conference on Computer Vision and Pattern Recognition*, 2024, pp. 5333–5343.

- [45] S. Zhou, H. Chang, S. Jiang, Z. Fan, Z. Zhu, D. Xu, P. Chari, S. You, Z. Wang, and A. Kadambi, "Feature 3DGS: Supercharging 3D Gaussian Splatting to Enable Distilled Feature Fields," in *Proceedings of the IEEE/CVF Conference on Computer Vision and Pattern Recognition*, 2024, pp. 21 676–21 685.
- [46] K. Cheng, X. Long, K. Yang, Y. Yao, W. Yin, Y. Ma, W. Wang, and X. Chen, "Gaussian Splatting with Progressive Propagation," in *Forty-first International Conference on Machine Learning*, 2024.
- [47] J. Chen, W. Ye, Y. Wang, D. Chen, D. Huang, W. Ouyang, G. Zhang, Y. Qiao, and T. He, "GigaGS: Scaling up Planar-Based 3D Gaussians for Large Scene Surface Reconstruction," arXiv preprint arXiv:2409.06685, 2024.
- [48] M. Qin, W. Li, J. Zhou, H. Wang, and H. Pfister, "LangSplat: 3D Language Gaussian Splatting," in Proceedings of the IEEE/CVF Conference on Computer Vision and Pattern Recognition, 2024, pp. 20051– 20060.
- [49] J. Zhang, F. Zhan, M. Xu, S. Lu, and E. Xing, "FreGS: 3D Gaussian Splatting with Progressive Frequency Regularization," in *Proceedings of the IEEE/CVF Conference on Computer Vision and Pattern Recognition*, 2024, pp. 21 424–21 433.
- [50] Z. Zeng, Y. Wang, L. Ju, and T. Guan, "Frequency-Aware Density Control via Reparameterization for High-Quality Rendering of 3D Gaussian Splatting," in *Proceedings of the AAAI Conference on Artificial Intelligence*, vol. 39, no. 9, 2025, pp. 9833–9841.
- [51] A. Knapitsch, J. Park, Q.-Y. Zhou, and V. Koltun, "Tanks and temples: Benchmarking large-scale scene reconstruction," *ACM Transactions on Graphics (ToG)*, vol. 36, no. 4, pp. 1–13, 2017.
- [52] P. Hedman, J. Philip, T. Price, J.-M. Frahm, G. Drettakis, and G. Brostow, "Deep blending for free-viewpoint image-based rendering," ACM Transactions on Graphics (ToG), vol. 37, no. 6, pp. 1–15, 2018.
- [53] Z. Wang, A. C. Bovik, H. R. Sheikh, and E. P. Simoncelli, "Image quality assessment: from error visibility to structural similarity," *IEEE transactions on image processing*, vol. 13, no. 4, pp. 600–612, 2004.
- [54] R. Zhang, P. Isola, A. A. Efros, E. Shechtman, and O. Wang, "The Unreasonable Effectiveness of Deep Features as a Perceptual Metric," in *Proceedings of the IEEE conference on computer vision and pattern recognition*, 2018, pp. 586–595.
- [55] K. Pearson, "Vii. note on regression and inheritance in the case of two parents," *proceedings of the royal society of London*, vol. 58, no. 347-352, pp. 240–242, 1895.
- [56] I. Sobel, G. Feldman et al., "A 3x3 isotropic gradient operator for image processing," a talk at the Stanford Artificial Project in, vol. 1968, pp. 271–272, 1968.
- [57] H. Scharr, "Optimal operators in digital image processing," 2000.
- [58] G. Shrivakshan and C. Chandrasekar, "A Comparison of various Edge Detection Techniques used in Image Processing," *International Journal of Computer Science Issues (IJCSI)*, vol. 9, no. 5, p. 269, 2012.

# **NeurIPS Paper Checklist**

The checklist is designed to encourage best practices for responsible machine learning research, addressing issues of reproducibility, transparency, research ethics, and societal impact. Do not remove the checklist: **The papers not including the checklist will be desk rejected.** The checklist should follow the references and follow the (optional) supplemental material. The checklist does NOT count towards the page limit.

Please read the checklist guidelines carefully for information on how to answer these questions. For each question in the checklist:

- You should answer [Yes], [No], or [NA].
- [NA] means either that the question is Not Applicable for that particular paper or the relevant information is Not Available.
- Please provide a short (1–2 sentence) justification right after your answer (even for NA).

The checklist answers are an integral part of your paper submission. They are visible to the reviewers, area chairs, senior area chairs, and ethics reviewers. You will be asked to also include it (after eventual revisions) with the final version of your paper, and its final version will be published with the paper.

The reviewers of your paper will be asked to use the checklist as one of the factors in their evaluation. While "[Yes]" is generally preferable to "[No]", it is perfectly acceptable to answer "[No]" provided a proper justification is given (e.g., "error bars are not reported because it would be too computationally expensive" or "we were unable to find the license for the dataset we used"). In general, answering "[No]" or "[NA]" is not grounds for rejection. While the questions are phrased in a binary way, we acknowledge that the true answer is often more nuanced, so please just use your best judgment and write a justification to elaborate. All supporting evidence can appear either in the main paper or the supplemental material, provided in appendix. If you answer [Yes] to a question, in the justification please point to the section(s) where related material for the question can be found.

# IMPORTANT, please:

- Delete this instruction block, but keep the section heading "NeurIPS Paper Checklist",
- · Keep the checklist subsection headings, questions/answers and guidelines below.
- Do not modify the questions and only use the provided macros for your answers.

#### 1. Claims

Question: Do the main claims made in the abstract and introduction accurately reflect the paper's contributions and scope?

Answer: [Yes]

Justification: We substantiate all the claims made in the abstract and introduction through corresponding experimental results.

# Guidelines:

- The answer NA means that the abstract and introduction do not include the claims made in the paper.
- The abstract and/or introduction should clearly state the claims made, including the contributions made in the paper and important assumptions and limitations. A No or NA answer to this question will not be perceived well by the reviewers.
- The claims made should match theoretical and experimental results, and reflect how much the results can be expected to generalize to other settings.
- It is fine to include aspirational goals as motivation as long as it is clear that these goals are not attained by the paper.

# 2. Limitations

Question: Does the paper discuss the limitations of the work performed by the authors?

Answer: [Yes]

Justification: We provide a discussion of the limitations of our method in Section5. Guidelines:

- The answer NA means that the paper has no limitation while the answer No means that the paper has limitations, but those are not discussed in the paper.
- The authors are encouraged to create a separate "Limitations" section in their paper.
- The paper should point out any strong assumptions and how robust the results are to violations of these assumptions (e.g., independence assumptions, noiseless settings, model well-specification, asymptotic approximations only holding locally). The authors should reflect on how these assumptions might be violated in practice and what the implications would be.
- The authors should reflect on the scope of the claims made, e.g., if the approach was only tested on a few datasets or with a few runs. In general, empirical results often depend on implicit assumptions, which should be articulated.
- The authors should reflect on the factors that influence the performance of the approach. For example, a facial recognition algorithm may perform poorly when image resolution is low or images are taken in low lighting. Or a speech-to-text system might not be used reliably to provide closed captions for online lectures because it fails to handle technical jargon.
- The authors should discuss the computational efficiency of the proposed algorithms and how they scale with dataset size.
- If applicable, the authors should discuss possible limitations of their approach to address problems of privacy and fairness.
- While the authors might fear that complete honesty about limitations might be used by reviewers as grounds for rejection, a worse outcome might be that reviewers discover limitations that aren't acknowledged in the paper. The authors should use their best judgment and recognize that individual actions in favor of transparency play an important role in developing norms that preserve the integrity of the community. Reviewers will be specifically instructed to not penalize honesty concerning limitations.

# 3. Theory assumptions and proofs

Question: For each theoretical result, does the paper provide the full set of assumptions and a complete (and correct) proof?

Answer: [Yes]

Justification: We present the complete set of assumptions in the introduction, outline the validation methodology in the Section method, and verify the correctness of our assumptions through experiments in experiments, especially in Section 4.3.

#### Guidelines:

- The answer NA means that the paper does not include theoretical results.
- All the theorems, formulas, and proofs in the paper should be numbered and cross-referenced.
- All assumptions should be clearly stated or referenced in the statement of any theorems.
- The proofs can either appear in the main paper or the supplemental material, but if they appear in the supplemental material, the authors are encouraged to provide a short proof sketch to provide intuition.
- Inversely, any informal proof provided in the core of the paper should be complemented by formal proofs provided in appendix or supplemental material.
- Theorems and Lemmas that the proof relies upon should be properly referenced.

# 4. Experimental result reproducibility

Question: Does the paper fully disclose all the information needed to reproduce the main experimental results of the paper to the extent that it affects the main claims and/or conclusions of the paper (regardless of whether the code and data are provided or not)?

Answer: [Yes]

Justification: We provide a detailed explanation of our method in the section method and describe the implementation details in Section 4.1.

#### Guidelines:

- The answer NA means that the paper does not include experiments.
- If the paper includes experiments, a No answer to this question will not be perceived well by the reviewers: Making the paper reproducible is important, regardless of whether the code and data are provided or not.
- If the contribution is a dataset and/or model, the authors should describe the steps taken to make their results reproducible or verifiable.
- Depending on the contribution, reproducibility can be accomplished in various ways. For example, if the contribution is a novel architecture, describing the architecture fully might suffice, or if the contribution is a specific model and empirical evaluation, it may be necessary to either make it possible for others to replicate the model with the same dataset, or provide access to the model. In general, releasing code and data is often one good way to accomplish this, but reproducibility can also be provided via detailed instructions for how to replicate the results, access to a hosted model (e.g., in the case of a large language model), releasing of a model checkpoint, or other means that are appropriate to the research performed.
- While NeurIPS does not require releasing code, the conference does require all submissions to provide some reasonable avenue for reproducibility, which may depend on the nature of the contribution. For example
- (a) If the contribution is primarily a new algorithm, the paper should make it clear how to reproduce that algorithm.
- (b) If the contribution is primarily a new model architecture, the paper should describe the architecture clearly and fully.
- (c) If the contribution is a new model (e.g., a large language model), then there should either be a way to access this model for reproducing the results or a way to reproduce the model (e.g., with an open-source dataset or instructions for how to construct the dataset).
- (d) We recognize that reproducibility may be tricky in some cases, in which case authors are welcome to describe the particular way they provide for reproducibility. In the case of closed-source models, it may be that access to the model is limited in some way (e.g., to registered users), but it should be possible for other researchers to have some path to reproducing or verifying the results.

#### 5. Open access to data and code

Question: Does the paper provide open access to the data and code, with sufficient instructions to faithfully reproduce the main experimental results, as described in supplemental material?

Answer: [Yes]

Justification: We use publicly available datasets described in Section4.1, and the code will be released in the future.

#### Guidelines:

- The answer NA means that paper does not include experiments requiring code.
- Please see the NeurIPS code and data submission guidelines (https://nips.cc/public/guides/CodeSubmissionPolicy) for more details.
- While we encourage the release of code and data, we understand that this might not be
  possible, so "No" is an acceptable answer. Papers cannot be rejected simply for not
  including code, unless this is central to the contribution (e.g., for a new open-source
  benchmark).
- The instructions should contain the exact command and environment needed to run to reproduce the results. See the NeurIPS code and data submission guidelines (https://nips.cc/public/guides/CodeSubmissionPolicy) for more details.
- The authors should provide instructions on data access and preparation, including how to access the raw data, preprocessed data, intermediate data, and generated data, etc.
- The authors should provide scripts to reproduce all experimental results for the new proposed method and baselines. If only a subset of experiments are reproducible, they should state which ones are omitted from the script and why.

- At submission time, to preserve anonymity, the authors should release anonymized versions (if applicable).
- Providing as much information as possible in supplemental material (appended to the paper) is recommended, but including URLs to data and code is permitted.

# 6. Experimental setting/details

Question: Does the paper specify all the training and test details (e.g., data splits, hyper-parameters, how they were chosen, type of optimizer, etc.) necessary to understand the results?

Answer: [Yes]

Justification: We specifically emphasize the experimental details in Section 4.1.

#### Guidelines:

- The answer NA means that the paper does not include experiments.
- The experimental setting should be presented in the core of the paper to a level of detail that is necessary to appreciate the results and make sense of them.
- The full details can be provided either with the code, in appendix, or as supplemental material.

#### 7. Experiment statistical significance

Question: Does the paper report error bars suitably and correctly defined or other appropriate information about the statistical significance of the experiments?

Answer: [Yes]

Justification: Although the variance has minimal impact in our experiments, we repeat each experiment three times and report the average to mitigate potential errors.

#### Guidelines:

- The answer NA means that the paper does not include experiments.
- The authors should answer "Yes" if the results are accompanied by error bars, confidence intervals, or statistical significance tests, at least for the experiments that support the main claims of the paper.
- The factors of variability that the error bars are capturing should be clearly stated (for example, train/test split, initialization, random drawing of some parameter, or overall run with given experimental conditions).
- The method for calculating the error bars should be explained (closed form formula, call to a library function, bootstrap, etc.)
- The assumptions made should be given (e.g., Normally distributed errors).
- It should be clear whether the error bar is the standard deviation or the standard error
  of the mean.
- It is OK to report 1-sigma error bars, but one should state it. The authors should preferably report a 2-sigma error bar than state that they have a 96% CI, if the hypothesis of Normality of errors is not verified.
- For asymmetric distributions, the authors should be careful not to show in tables or figures symmetric error bars that would yield results that are out of range (e.g. negative error rates).
- If error bars are reported in tables or plots, The authors should explain in the text how they were calculated and reference the corresponding figures or tables in the text.

# 8. Experiments compute resources

Question: For each experiment, does the paper provide sufficient information on the computer resources (type of compute workers, memory, time of execution) needed to reproduce the experiments?

Answer: [Yes]

Justification: We specify in Section4.1 that our experiments were conducted using an NVIDIA 3090 GPU.

Guidelines:

- The answer NA means that the paper does not include experiments.
- The paper should indicate the type of compute workers CPU or GPU, internal cluster, or cloud provider, including relevant memory and storage.
- The paper should provide the amount of compute required for each of the individual experimental runs as well as estimate the total compute.
- The paper should disclose whether the full research project required more compute than the experiments reported in the paper (e.g., preliminary or failed experiments that didn't make it into the paper).

#### 9. Code of ethics

Question: Does the research conducted in the paper conform, in every respect, with the NeurIPS Code of Ethics https://neurips.cc/public/EthicsGuidelines?

Answer: [Yes]

Justification: Our research complies with the NeurIPS Code of Ethics in all respects.

#### Guidelines:

- The answer NA means that the authors have not reviewed the NeurIPS Code of Ethics.
- If the authors answer No, they should explain the special circumstances that require a
  deviation from the Code of Ethics.
- The authors should make sure to preserve anonymity (e.g., if there is a special consideration due to laws or regulations in their jurisdiction).

#### 10. **Broader impacts**

Question: Does the paper discuss both potential positive societal impacts and negative societal impacts of the work performed?

Answer: [NA]

Justification: Our research focuses on reconstructing real-world scenes and does not involve any direct societal impact.

#### Guidelines:

- The answer NA means that there is no societal impact of the work performed.
- If the authors answer NA or No, they should explain why their work has no societal impact or why the paper does not address societal impact.
- Examples of negative societal impacts include potential malicious or unintended uses (e.g., disinformation, generating fake profiles, surveillance), fairness considerations (e.g., deployment of technologies that could make decisions that unfairly impact specific groups), privacy considerations, and security considerations.
- The conference expects that many papers will be foundational research and not tied to particular applications, let alone deployments. However, if there is a direct path to any negative applications, the authors should point it out. For example, it is legitimate to point out that an improvement in the quality of generative models could be used to generate deepfakes for disinformation. On the other hand, it is not needed to point out that a generic algorithm for optimizing neural networks could enable people to train models that generate Deepfakes faster.
- The authors should consider possible harms that could arise when the technology is being used as intended and functioning correctly, harms that could arise when the technology is being used as intended but gives incorrect results, and harms following from (intentional or unintentional) misuse of the technology.
- If there are negative societal impacts, the authors could also discuss possible mitigation strategies (e.g., gated release of models, providing defenses in addition to attacks, mechanisms for monitoring misuse, mechanisms to monitor how a system learns from feedback over time, improving the efficiency and accessibility of ML).

# 11. Safeguards

Question: Does the paper describe safeguards that have been put in place for responsible release of data or models that have a high risk for misuse (e.g., pretrained language models, image generators, or scraped datasets)?

Answer: [NA]

Justification: Our research focuses on reconstructing real-world scenes and does not involve high risk for misuse.

#### Guidelines:

- The answer NA means that the paper poses no such risks.
- Released models that have a high risk for misuse or dual-use should be released with
  necessary safeguards to allow for controlled use of the model, for example by requiring
  that users adhere to usage guidelines or restrictions to access the model or implementing
  safety filters.
- Datasets that have been scraped from the Internet could pose safety risks. The authors should describe how they avoided releasing unsafe images.
- We recognize that providing effective safeguards is challenging, and many papers do
  not require this, but we encourage authors to take this into account and make a best
  faith effort.

#### 12. Licenses for existing assets

Question: Are the creators or original owners of assets (e.g., code, data, models), used in the paper, properly credited and are the license and terms of use explicitly mentioned and properly respected?

Answer: [Yes]

Justification: We properly cite all the sources of the existing assets used in our work in the references.

#### Guidelines:

- The answer NA means that the paper does not use existing assets.
- The authors should cite the original paper that produced the code package or dataset.
- The authors should state which version of the asset is used and, if possible, include a URL.
- The name of the license (e.g., CC-BY 4.0) should be included for each asset.
- For scraped data from a particular source (e.g., website), the copyright and terms of service of that source should be provided.
- If assets are released, the license, copyright information, and terms of use in the package should be provided. For popular datasets, paperswithcode.com/datasets has curated licenses for some datasets. Their licensing guide can help determine the license of a dataset.
- For existing datasets that are re-packaged, both the original license and the license of the derived asset (if it has changed) should be provided.
- If this information is not available online, the authors are encouraged to reach out to the asset's creators.

#### 13. New assets

Question: Are new assets introduced in the paper well documented and is the documentation provided alongside the assets?

Answer: [NA]

Justification: Our work does not involve the release of any new assets.

#### Guidelines:

- The answer NA means that the paper does not release new assets.
- Researchers should communicate the details of the dataset/code/model as part of their submissions via structured templates. This includes details about training, license, limitations, etc.
- The paper should discuss whether and how consent was obtained from people whose asset is used.
- At submission time, remember to anonymize your assets (if applicable). You can either create an anonymized URL or include an anonymized zip file.

#### 14. Crowdsourcing and research with human subjects

Question: For crowdsourcing experiments and research with human subjects, does the paper include the full text of instructions given to participants and screenshots, if applicable, as well as details about compensation (if any)?

Answer: [NA]

Justification: Our research does not involve crowdsourcing experiments or studies with human subjects.

# Guidelines:

- The answer NA means that the paper does not involve crowdsourcing nor research with human subjects.
- Including this information in the supplemental material is fine, but if the main contribution of the paper involves human subjects, then as much detail as possible should be included in the main paper.
- According to the NeurIPS Code of Ethics, workers involved in data collection, curation, or other labor should be paid at least the minimum wage in the country of the data collector.

# 15. Institutional review board (IRB) approvals or equivalent for research with human subjects

Question: Does the paper describe potential risks incurred by study participants, whether such risks were disclosed to the subjects, and whether Institutional Review Board (IRB) approvals (or an equivalent approval/review based on the requirements of your country or institution) were obtained?

Answer: [NA]

Justification: The paper does not involve related research.

#### Guidelines:

- The answer NA means that the paper does not involve crowdsourcing nor research with human subjects.
- Depending on the country in which research is conducted, IRB approval (or equivalent) may be required for any human subjects research. If you obtained IRB approval, you should clearly state this in the paper.
- We recognize that the procedures for this may vary significantly between institutions and locations, and we expect authors to adhere to the NeurIPS Code of Ethics and the guidelines for their institution.
- For initial submissions, do not include any information that would break anonymity (if applicable), such as the institution conducting the review.

# 16. Declaration of LLM usage

Question: Does the paper describe the usage of LLMs if it is an important, original, or non-standard component of the core methods in this research? Note that if the LLM is used only for writing, editing, or formatting purposes and does not impact the core methodology, scientific rigorousness, or originality of the research, declaration is not required.

Answer: [NA]

Justification: All the content in our paper is written by ourselves and does not involve the use of LLMs.

# Guidelines:

- The answer NA means that the core method development in this research does not involve LLMs as any important, original, or non-standard components.
- Please refer to our LLM policy (https://neurips.cc/Conferences/2025/LLM) for what should or should not be described.

# **Appendix**

# **A** Impletation Details

#### A.1 Algorithmic Implementation of CDC-GS

Algorithm 1 provides a detailed pseudocode of the training pipeline in CDC-GS. Built upon the vanilla 3DGS [1] framework, our procedure starts from a sparse initialization of Gaussian primitives and proceeds with joint optimization and CDC-guided density control across iterations. This pseudocode comprehensively implements the pipeline described in Section 3 of the main paper, integrating both loss-driven and prior-based cues for efficient and high-fidelity Gaussian allocation.

## A.2 Haar-based DWT Implementation

In our method, the visual complexity of each training view is extracted using a single-level 2D Discrete Wavelet Transform (DWT)[9]. We adopt the Haar wavelet basis due to its simplicity and efficiency. The filtering process is separable and implemented as two 1D convolutions along height and width, as defined in Equation 3 of the main paper, where  $F_L = [1,1]/\sqrt{2}$ ,  $F_H = [-1,1]/\sqrt{2}$  are the 1D low-pass and high-pass Haar filters. The resulting four subbands correspond to different frequency directions. Each 2D kernel derived from outer products of filters is summarized in Table 3.

Table 3: 2D Haar DWT convolution kernels derived from filter outer products.

Subband	LI	_	LH		Н	_	НН			
Kernel K	$\frac{1}{2} \begin{bmatrix} 1 \\ 1 \end{bmatrix}$	1 1	$\frac{1}{2} \begin{bmatrix} -1 \\ -1 \end{bmatrix}$	1 1	$\frac{1}{2} \begin{bmatrix} -1 \\ 1 \end{bmatrix}$	$\begin{bmatrix} -1 \\ 1 \end{bmatrix}$	$\frac{1}{2} \begin{bmatrix} 1 \\ -1 \end{bmatrix}$	$\begin{bmatrix} -1 \\ 1 \end{bmatrix}$		

To compute the visual complexity of each image, we construct a high-pass filter by discarding the non-directional low-frequency subband  $I^{\rm LL}$ , and reconstruct the complexity map as defined in Equation 4 of the main paper. This effectively preserves only the high-frequency directional responses (vertical, horizontal and diagonal), enabling the resulting map E to serve as a spatially-varying representation of complexity.

# **B** More Ablations

# **B.1** Comparison to Classical High-Pass Filters

To validate the effectiveness of our DWT-based design, we replace our DWT-based frequency estimation with three classical high-pass filters: Sobel[56], Scharr[57] and Laplacian[58], defined in Table 4, then integrate each into the CDC-GS framework without any other modifications.

Table 4: High-pass filter kernels used for comparison.

Sobel	Scharr	Laplacian				
	$K_x = \begin{bmatrix} -3 & 0 & 3 \\ -10 & 0 & 10 \\ -3 & 0 & 3 \end{bmatrix}$ $K_y = \begin{bmatrix} -3 & -10 & -3 \\ 0 & 0 & 0 \\ 3 & 10 & 3 \end{bmatrix}$	$K = \begin{bmatrix} 0 & -1 & 0 \\ -1 & 4 & -1 \\ 0 & -1 & 0 \end{bmatrix}$				

As shown in Table 5, all methods achieve similar performance in rendering quality, demonstrating the robustness of our CDC-GS framework to the choice of complexity estimator. Notably, the DWT-based variant slightly outperforms the others in both rendering quality and Gaussian compactness. We

# Algorithm 1 CDC-GS Optimization and Density Control

```
Input: w, h: width and height of the training images
 1: M \leftarrow SfM Points
                                                                                                                                    ▶ Positions
 2: S, C, A \leftarrow InitAttributes()
                                                                                                   3: i \leftarrow 0
                                                                                                                           ▶ Iteration Count
 4: (I^{\text{LL}}, I^{\text{LH}}, I^{\text{HL}}, I^{\text{HH}}) \leftarrow \text{DWT}(I)
5: E \leftarrow \text{IDWT}(0, I^{\text{LH}}, I^{\text{HL}}, I^{\text{HH}})
                                                                                                                                           ⊳ Eq.3
                                                                                                                                           ⊳ Eq.4
 6: while not converged do

ightharpoonup Camera V and Image I
         V, I \leftarrow SampleTrainingView()
 7:
         \tilde{I} \leftarrow \text{Rasterize}(M, S, C, A, V)
                                                                                                                      \triangleright Rendered Image \tilde{I}
 8:
 9:
         L \leftarrow \text{Loss}(I, I)

    Loss

10:
         M, S, C, A \leftarrow \operatorname{Adam}(\nabla L)

⊳ Backprop & Step

11:
         if IsRefinementIteration(i) then
12:
             \Gamma \leftarrow \text{Complexity}(M, S, C, A, E)
                                                                                                                                           ⊳ Eq.5
13:
             \Psi \leftarrow \text{Density}(M, S, C, A)
                                                                                                                                           ⊳ Eq.6
14:
             s_i \leftarrow \text{ConsistencyScore}(\Gamma, \Psi)
                                                                                                                                           ⊳ Eq.7
15:
             Compute sampling probabilities:
                 p_{i}^{\mathrm{dens}} \propto |s_i| \text{ if } \Gamma_i > \mu_{\Gamma}, \Psi_i < \mu_{\Psi}
16:
                                                                                                    ▶ High-complexity, Low-density
                 p_i^{\text{prune}} \propto \alpha_i \text{ if } \Gamma_i < \mu_{\Gamma}, \Psi_i > \mu_{\Psi}
                                                                                                    17:
             \begin{array}{l} \text{Sample } \mathcal{M}_{\text{cdc\_densify}} \sim \text{Multinomial}(p^{\text{dens}}, \rho_d \cdot N) \\ \text{Sample } \mathcal{M}_{\text{cdc\_prune}} \sim \text{Multinomial}(p^{\text{prune}}, \rho_p \cdot N) \end{array}
18:
19:
             for all Gaussians (\mu, \Sigma, c, \alpha) in (M, S, C, A) do
20:
21:
                 if (\mu, \Sigma, c, \alpha) \in \mathcal{M}_{cdc\_prune} then
22:
                     RemoveGaussian(\mu, \Sigma, c, \alpha)
                                                                                                                              23:
                 end if
                 if (i \mod 3000 = 0) and (\alpha < 0.1) then
24:
                     RemoveGaussian(\mu, \Sigma, c, \alpha)
25:
                                                                                                                         ▶ Periodic Pruning
                 end if
26:
27:
                 \tau(\Gamma) \leftarrow AdaptiveThreshold(\Gamma)
                                                                                                                                           ⊳ Eq.8
28:
                 \mathcal{M}_{\text{loss}} \leftarrow \{G_i \mid \nabla_p L_i > \tau(\Gamma_i)\}
                                                                                                                           \mathcal{M}_{\text{densify}} \leftarrow \mathcal{M}_{\text{loss}} \cup \mathcal{M}_{\text{cdc\_densify}}
29:
                 if (\mu, \Sigma, c, \alpha) \in \mathcal{M}_{densify} then
30:
                     if \|\Sigma\| > \tau_s then
31:
                         SplitGaussian(\mu, \Sigma, c, \alpha)
32:
                                                                                                                     ▷ Over-reconstruction
33:
                     else
                         CloneGaussian(\mu, \Sigma, c, \alpha)
34:
                                                                                                                   35:
                     end if
                 end if
36:
37:
             end for
38:
         end if
         i \leftarrow i + 1
39:
40: end while
41: return Optimized Gaussian primitives (M, S, C, A)
```

attribute this to the multi-scale and multi-directional nature of the DWT, which enables more accurate modeling of visual complexity.

# **B.2** Geometric vs. Arithmetic Mean

In Table 6, we compare two variants of our CDC-GS framework that differ only in how they compute the density of Gaussian primitives. Specifically, the Arithmetic Mean variant uses the inverse of the arithmetic mean of distances to neighboring Gaussians, whereas the Geometric Mean variant (our default, as defined in Equation 6 of the main paper) adopts the geometric mean formulation. Both variants are evaluated under identical settings.

Results show that using the geometric mean consistently yields slightly better rendering quality and reduces the number of Gaussians across all benchmarks. This confirms our choice, as the geometric

Table 5: Comparison to classical high-pass filters on MipNeRF 360 [30]. We replace our DWT-based complexity estimation with Sobel, Scharr and Laplacian filters to construct complexity maps for CDC-GS. Our DWT-based formulation achieves the best performance across all metrics.

Filter	PSNR ↑	SSIM ↑	LPIPS ↓	#GS↓
Sobel	27.96	0.834	0.186	2.60M
Scharr	27.97	0.835	0.186	2.59M
Laplacian	27.96	0.835	0.184	2.54M
DWT	<b>28.02</b>	<b>0.836</b>	<b>0.183</b>	2.53M

mean provides a more sensitive estimation of local density, especially for short distances. We adopt the geometric mean formulation throughout the main paper.

Table 6: **Geometric vs. Arithmetic Mean in density computation.** We compare two variants of CDC-GS that differ only in whether the geometric or arithmetic mean is used for density estimation. The geometric mean consistently yields better performance with fewer Gaussians.

Method	]	MipNeRF	360[30]		Ta	anks & Te	emples[51]	1	Deep Blending[52]				
	PSNR ↑	SSIM $\uparrow$	LPIPS ↓	#GS ↓	PSNR ↑	SSIM ↑	LPIPS ↓	#GS ↓	PSNR ↑	SSIM ↑	LPIPS ↓	#GS ↓	
Arithmetic Geometric		0.834 <b>0.836</b>	0.185 <b>0.183</b>			0.862 <b>0.866</b>			29.82 <b>29.83</b>	0.909 0.909	0.234 0.234		

# **B.3** Reverse-CDC Ablation

To further examine the role of complexity–density alignment, we designed a reverse variant in which Gaussians are densified in low-complexity & high-density regions and pruned in high-complexity & low-density ones, thereby inverting the CDC guidance.

Table 7: **Reverse-CDC ablation on MipNeRF 360 [30]**. Comparing vanilla 3DGS with Reverse-CDC shows degraded quality and increased number of Gaussians, highlighting the necessity of complexity–density alignment.

Method	PSNR ↑	SSIM $\uparrow$	LPIPS $\downarrow$	#GS↓
3DGS Reverse-CDC	<b>27.79</b> 27.62	<b>0.826</b> 0.817	<b>0.201</b> 0.224	<b>2.59M</b> 2.71M

As shown in Table 7, this reverse allocation leads to a degradation in rendering quality and a larger number of Gaussians. Although more primitives are introduced, the reconstruction becomes worse, demonstrating that enforcing complexity–density alignment is essential for efficient modeling.

# **B.4** Efficiency Analysis of CDC-GS

We summarize the additional training cost introduced by the complexity and density modules. As shown in Table 8, the average overhead is dominated by the wavelet-based complexity computation, whereas both modules benefit from CUDA acceleration, keeping the cost practical. Although the training time increases, the rendering speed remains identical to vanilla 3DGS, and CDC-GS achieves higher reconstruction quality with a moderate additional cost.

# C Additional Experiment Results

#### C.1 Extended Visualization of Complexity-Density Correlation

As a supplement to the consistency analysis in Section 4.3 of the main paper, we provide additional visualizations of the complexity-density correlation variation on three scenes from different datasets: the outdoor scene "garden" from MipNeRF 360 [30], "train" from Tanks & Temples [51], and indoor

Table 8: **Training efficiency analysis of CDC-GS components on MipNeRF 360 [30].** "+ Density Only" and "+ Complexity Only" denote adding the KNN- and DWT-based modules individually.

Method Variant	Training Time	Overhead
3DGS (baseline)	29:06	-
+ Density Only (KNN)	30:40	+1:34
+ Complexity Only (DWT)	33:19	+4:13
CDC-GS (Full, Ours 0.01)	35:36	+6:30

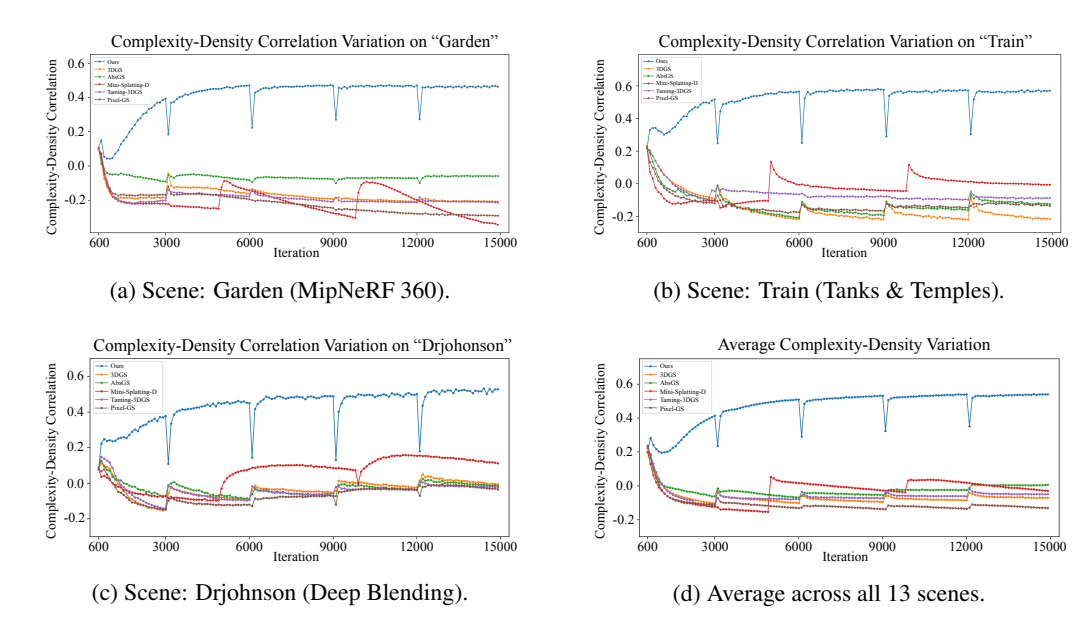


Figure 6: Complexity-density correlation variation across datasets. We show the Pearson correlation between visual complexity and local primitive density over training iterations. Our CDC-GS consistently improves and maintains this correlation, indicating stronger structural consistency compared to baseline methods.

scene "drjohnson" from Deep Blending [52]. We also report the average correlation variation across all 13 evaluated scenes.

These results in Figure 6 further validate the robustness of our CDC-GS framework in aligning visual complexity with local density across different scenes and datasets. In contrast, baseline methods often show unstable correlation trends or even negative correlation values, which contradict the expected relationship between structural complexity and spatial density, leading to persistent under-reconstruction in complex regions and over-reconstruction in simple areas.

# **C.2** Supplementary Qualitative Results

As presented in Tables 9–12, our CDC-GS method consistently outperforms baselines across diverse benchmarks in terms of PSNR, SSIM, and LPIPS, while maintaining a significantly lower or comparable number of Gaussians. Specifically, under the same or fewer primitives, CDC-GS achieves better fidelity in high-complexity, detail-rich regions, thanks to its frequency-guided complexity modeling. This highlights the effectiveness of our complexity-density consistency strategy in allocating primitives to structurally complex areas, offering a complementary and orthogonal benefit to existing loss-driven methods. Our approach proves especially advantageous under constrained Gaussian budgets, delivering improved rendering quality without sacrificing efficiency.

Table 9: **Per-scene PSNR scores across three datasets. Bold** indicates the best results. Our method consistently achieves competitive or superior results across diverse scenes.

Method		MipNeRF 360[30]									Temples[51]	Deep Ble	Deep Blending[52]	
	Flowers	Treehill	Garden	Bicycle	Stump	Kitchen	Bonsai	Counter	Room	Train	Truck	Drjohnson	Playroom	
3DGS[1]	21.92	22.86	27.88	25.68	26.91	31.42	32.47	29.18	31.81	22.07	25.51	29.37	30.09	
Taming-3DGS[8]	21.81	23.08	27.78	25.47	26.63	32.05	32.84	29.38	32.12	22.62	26.01	29.43	30.03	
Ours (0.01)	22.01	22.69	28.14	25.96	27.13	32.18	32.32	29.41	32.37	22.61	26.22	29.61	30.06	
AbsGS[4]	21.78	22.19	27.87	25.76	27.04	31.48	32.32	29.18	31.87	21.14	25.30	28.61	29.96	
Mini-Splatting-D[3]	21.89	22.59	27.80	26.00	27.46	31.48	32.35	28.62	31.83	21.22	25.39	29.40	30.47	
Pixel-GS[5]	21.94	22.52	27.88	25.72	27.18	31.92	32.60	29.29	31.46	21.89	25.44	28.08	29.82	
Ours (0.02)	22.14	22.74	28.26	25.99	27.39	32.25	32.38	29.51	32.33	22.74	26.19	29.68	30.39	

Table 10: **Per-scene SSIM scores across three datasets. Bold** indicates the best results. Our method consistently achieves competitive or superior results across diverse scenes.

Method				MipN		Tanks & Temples[51]		Deep Ble	nding[52]				
	Flowers	Treehill	Garden	Bicycle	Stump	Kitchen	Bonsai	Counter	Room	Train	Truck	Drjohnson	Playroom
3DGS[1]	0.622	0.652	0.875	0.779	0.783	0.933	<b>0.948</b>	0.916	0.929	0.820	0.885	0.905	0.907
Taming-3DGS[8]	0.613	0.646	0.871	0.775	0.771	0.930	0.946	0.910	0.922	0.831	0.893	0.908	0.908
Ours (0.01)	<b>0.648</b>	<b>0.656</b>	<b>0.883</b>	<b>0.801</b>	<b>0.794</b>	<b>0.936</b>	0.947	<b>0.921</b>	<b>0.936</b>	<b>0.837</b>	<b>0.895</b>	<b>0.908</b>	<b>0.911</b>
AbsGS[4]	0.654	0.645	0.883	0.801	0.795	0.935	0.951	0.920	0.935	0.822	0.890	0.899	0.907
Mini-Splatting-D[3]	0.659	0.659	0.884	<b>0.811</b>	<b>0.816</b>	0.936	<b>0.953</b>	0.918	0.936	0.819	0.890	0.906	0.908
Pixel-GS[5]	0.653	0.652	0.879	0.792	0.798	0.936	0.952	0.922	0.930	0.825	0.887	0.887	0.905
Ours (0.02)	<b>0.660</b>	<b>0.660</b>	<b>0.887</b>	0.808	0.812	<b>0.938</b>	0.947	<b>0.925</b>	<b>0.940</b>	<b>0.838</b>	<b>0.895</b>	<b>0.912</b>	<b>0.912</b>

Table 11: **Per-scene LPIPS scores across three datasets. Bold** indicates the best results. Our method consistently achieves competitive or superior results across diverse scenes.

Method		MipNeRF 360[30]									Tanks & Temples[51]		Deep Blending[52]	
	Flowers	Treehill	Garden	Bicycle	Stump	Kitchen	Bonsai	Counter	Room	Train	Truck	Drjohnson	Playroom	
3DGS[1]	0.328	0.316	0.102	0.203	0.209	0.113	0.173	0.178	0.191	0.197	0.142	0.236	0.240	
Taming-3DGS[8]	0.334	0.310	0.104	0.200	0.212	0.126	0.196	0.200	0.217	0.190	0.123	0.233	0.235	
Ours (0.01)	0.274	0.289	0.090	0.175	0.206	0.109	0.165	0.167	0.170	0.181	0.118	0.232	0.235	
AbsGS[4]	0.244	0.256	0.089	0.157	0.182	0.106	0.155	0.162	0.168	0.182	0.122	0.236	0.229	
Mini-Splatting-D[3]	0.246	0.256	0.086	0.151	0.163	0.105	0.142	0.152	0.162	0.181	0.100	0.218	0.203	
Pixel-GS[5]	0.252	0.270	0.093	0.173	0.180	0.106	0.161	0.162	0.183	0.179	0.120	0.255	0.240	
Ours (0.02)	0.240	0.256	0.085	0.154	0.169	0.104	0.155	0.153	0.162	0.171	0.108	0.220	0.216	

Table 12: **Per-scene number of Gaussian primitives across three datasets.** Values are reported in millions; **bold** indicates the lowest per scene. Our CDC-GS achieves competitive or significantly lower primitive counts, demonstrating its superior efficiency.

Method				MipN		Tanks & Temples[51]		Deep Blending[52]					
	Flowers	Treehill	Garden	Bicycle	Stump	Kitchen	Bonsai	Counter	Room	Train	Truck	Drjohnson	Playroom
3DGS[1] Taming-3DGS[8] Ours (0.01)	<b>2.75M</b> 3.09M 3.09M		3.62M	4.42M	3.92M	0.94M	1.00M	1.04M <b>0.82M</b> <b>0.82M</b>	1.07M		2.05M 2.07M 2.07M	3.11M 2.53M 2.53M	1.84M 1.60M 1.60M
AbsGS[4] Mini-Splatting-D[3] Pixel-GS[5] Ours (0.02)	5.16M <b>4.76M</b> 7.10M 5.14M	<b>4.83M</b> 7.47M	5.44M 7.64M	<b>5.85M</b> 8.59M	<b>5.30M</b> 6.49M	3.69M 3.05M	3.76M 2.06M	1.49M 3.83M 2.50M 1.33M	4.06M 2.49M	3.95M	2.16M 4.58M 5.21M 3.34M	4.04M 4.91M 5.55M <b>3.09M</b>	2.22M 4.35M 3.74M <b>1.89M</b>